



ELSEVIER

Surface Science 515 (2002) 453–461



www.elsevier.com/locate/susc

# How does a multiwalled carbon nanotube atomic force microscopy probe affect the determination of surface roughness statistics?

Q.M. Hudspeth<sup>a,\*</sup>, K.P. Nagle<sup>b</sup>, Y.-P. Zhao<sup>a</sup>, T. Karabacak<sup>a</sup>, C.V. Nguyen<sup>c,d</sup>,  
M. Meyyappan<sup>c</sup>, G.-C. Wang<sup>a</sup>, T.-M. Lu<sup>a</sup>

<sup>a</sup> Department of Physics, Applied Physics and Astronomy, Rensselaer Polytechnic Institute, 110 Eighth Street, Troy, NY 12180-3590, USA

<sup>b</sup> Department of Physics, Middlebury College, Middlebury, VT 05753, USA

<sup>c</sup> NASA Ames Research Center, MS229-1, Moffett Field, CA 94035, USA

<sup>d</sup> ELORET Corporation, 690 W. Fremont Ave, Sunnyvale, CA 94087, USA

Received 18 March 2002; accepted for publication 6 May 2002

## Abstract

Through statistical analysis of atomic force micrographs of sputtered-silicon films, we examine the determination of surface roughness parameters, and how this determination is affected by probe characteristics, such as sharpness and aspect ratio. We compare values for the roughness exponent,  $\alpha$ , and the lateral correlation length,  $\xi$ , calculated from micrographs obtained with multiple standard atomic force microscopy (AFM) probes in contact and noncontact modes, as well as from micrographs obtained with a multiwalled-nanotube-enhanced AFM probe. The sharper, lower-aspect-ratio nanotube probe is expected to provide a truer picture of the roughness parameters for these films. Using the nanotube probe, we obtained  $\alpha = 0.61 \pm 0.02$ , as compared to  $\alpha \sim 0.83$  obtained with conventional probes. We have also found the nanotube probe is able to detect a smaller lateral correlation length compared to that of the conventional AFM probes.

© 2002 Elsevier Science B.V. All rights reserved.

**Keywords:** Carbon; Atomic force microscopy; Surface roughening; Dendritic and/or fractile surfaces

## 1. Introduction

The phenomenon of growth-/etch-front roughening occurs far from equilibrium and is a subject of great interest for the fundamental understanding of growth/etch mechanisms [1–3]. The basic

methodology used to study roughening evolution is to quantitatively measure the growth/etch roughness parameters, such as roughness exponent,  $\alpha$ , and lateral correlation length,  $\xi$ . These parameters can be extracted from the equal-time height–height correlation function,  $H(\mathbf{r}, t)$ , defined as  $H(\mathbf{r}) = \langle [h(\mathbf{r}) - h(\mathbf{0})]^2 \rangle$ , and the autocovariance function,  $G(\mathbf{r})$ , defined as  $G(\mathbf{r}) = \langle [h(\mathbf{r})h(\mathbf{0})] \rangle$ . Here  $h(\mathbf{r})$  is the surface height at position  $\mathbf{r}$  on the surface, and the notation,  $\langle \cdot \cdot \cdot \rangle$ , indicates a statistical

\* Corresponding author. Tel.: +1-518-276-8418; fax: +1-518-276-6680.

E-mail address: [hudspq@rpi.edu](mailto:hudspq@rpi.edu) (Q.M. Hudspeth).

average. For a homogeneous, isotropic surface,  $H(\mathbf{r})$  and  $G(\mathbf{r})$  depend only on the distance,  $r$ , between two points, and the scalar notation  $H(r)$  and  $G(r)$  is used. Usually, a self-affine scaling hypothesis is also assumed, such that  $H(r) = \rho^2 r^{2\alpha}$ , for  $r \ll \xi$ , and  $H(r) = 2w^2$ , for  $r \gg \xi$  [4]. Here  $\rho$  is the average local slope,  $\alpha$  is the roughness exponent, a description of the surface fractality, and  $w$  is the interface width, or rms roughness.

By comparing the experimentally extracted parameters,  $\alpha$ , and  $\xi$ , and their time dependencies with those predicted by theory, considerable progress has been made in the basic understanding of the growth/etch phenomena [1–3]. In order to further this progress, it is necessary to obtain ever more accurate statistical information about surface morphologies associated with different growth/etch mechanisms. In this paper, we address the issue of pushing the limits of measurement accuracy using unconventional probes.

There are two basic experimental techniques used to obtain surface roughness parameters: diffraction and real-space imaging. Diffraction is an indirect technique and requires modeling to extract the roughness parameters, while real-space imaging provides direct, topographical images of a surface [4]. Among the real-space imaging techniques, atomic force microscopy (AFM) is widely used to image surface morphologies of various kinds of material surfaces. Since AFM employs a finite sized, physical probe to scan across the surface, the resolution of the probe is a determining factor in the accuracy of extracted roughness parameters.

Theoretical studies have shown that the resolution of AFM images is limited by several factors, including the sharpness of the cantilever tip [5,6]. Two important parameters determine the quality of an AFM tip: the tip diameter,  $d$ , and the aspect ratio of the tip,  $\gamma$  (defined for congruence with Ref. [6] to be  $\gamma = \text{diameter}/\text{length}$ ). A good tip requires both small  $d$  and small  $\gamma$ . Aué and De Hosson [6] have performed a detailed numerical experiment regarding the effect of AFM tip aspect ratios on the determination of a surface's local fractal dimension,  $D_s$ . According to their calculations, using a tip with  $\gamma \sim 0.35$ –1.15, one would underestimate a fractal surface with  $D_s = 1.5$  to have  $D_s \sim 1.3$ .

The authors further suggest that aspect ratios of at most 0.05 would be necessary to reduce the distortion to acceptable levels. Due to the underestimation of  $D_s$ , one would overestimate a surface with  $\alpha = 0.5$  to have  $\alpha \sim 0.7$ , because  $\alpha = 3 - D_s$ . As  $\alpha$  is constrained to lie between zero and one, this difference of 0.2 in  $\alpha$  can have a significant impact on the determination of a growth/etch mechanism.

For many years, the sharpest commercially available AFM tips have had  $d \sim 10$  nm,  $\gamma \sim 0.35$ , and provided a lateral resolution of 1–2 nm (for extremely flat surfaces) [7–9]. Recently, two responses to this situation have arisen. There are now a few low aspect ratio (small  $\gamma$ ) AFM probes commercially available that consist of fine silicon spikes with  $\gamma \sim 0.1$  [10]. In addition, in the past few years, the attachment of multiwalled nanotubes (MWNT) to conventional AFM tips has led to a great advancement in the spatial resolution of AFM images, as well as the long-term robustness of the probe [11–14]. While much work has touted the enhancement of lateral resolution offered by nanotube-enhanced AFM tips (tube-tips), little has been done to examine the quantitative advantages of tube-tips as seen through surface statistics.

The ability of a low aspect ratio nanotube to image deep, narrow cracks should have a great effect on the determination of  $\alpha$  and  $\xi$ , which depend on both lateral and vertical resolution [4]. In this

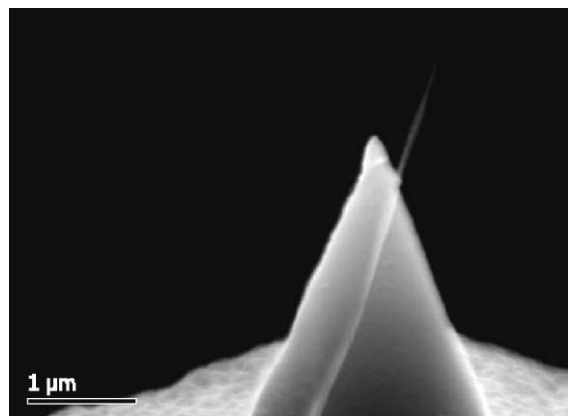


Fig. 1. An SEM image of the MWNT probe used in these experiments.

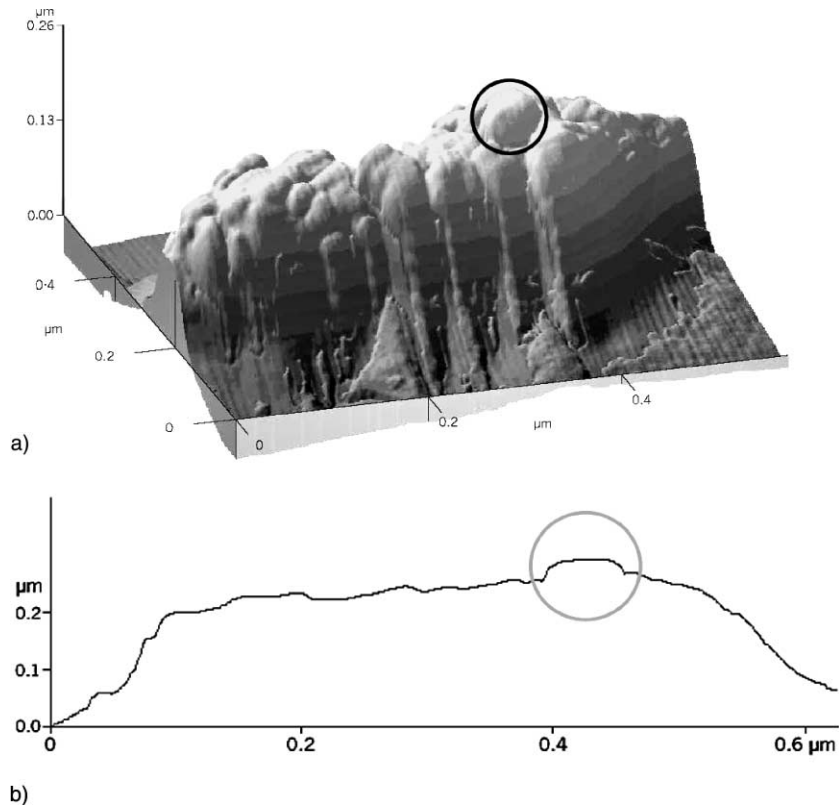


Fig. 2. Micrograph of a silicon characterization spike imaged with a Si-tip. (a) A 3-D projection of the topography. The black circle highlights the tallest region of the scan, which is associated with the nominal scanning region of the Si-tip. (b) A cross-section of the topography shown in (a). The gray circle highlights the region circled in (a).

paper, we present an experimental study of how the tip quality, as measured by  $d$  and  $\gamma$ , affects the determination of  $\alpha$  and  $\xi$ . We compare AFM images of a series of sputtered-silicon films obtained with conventional AFM probes (Si-tip and  $\text{Si}_3\text{N}_4$ -tip) and an MWNT-enhanced probe (tube-tip).

## 2. Characterization of MWNT tip

A simple and efficient process is used to fabricate the tube-tip. First, a cartridge containing nanotubes is prepared using chemical vapor deposition. Then, a single nanotube is transferred to the tip of the cantilever using an electric field. This process allows a single nanotube to be used as a probe, instead of a bundle. Detailed fabrication procedures are described elsewhere [15,16]. Fig. 1 shows

a scanning electron microscope (SEM) image of the tube-tip used in this study. The MWNT extends  $\sim 600$  nm beyond the apex of the silicon pyramid, and has a diameter that is vanishingly small at the resolution of this image ( $\sim 45$  nm) corresponding to an overall aspect ratio of  $\gamma = 0.075$ . After mounting the MWNT to its carrier tip, we observed a lateral scanning resolution of  $\sim 5$  nm.<sup>1</sup> To further characterize both the Si-tip and the tube-tip, a standard tip-characterization grating (MikroMasch grating TGT01), consisting of an array of sharpened silicon spikes of tip-curvature

<sup>1</sup> Resolution of the tube-tip was determined by cross-sectional analysis of micrographs of iridium particles deposited on mica. The iridium was an  $\sim 2$  nm thick ion-beam-sputter-deposited film. Though the distribution of particle sizes was large, particles as small as 5 nm were resolved.

radius  $<10$  nm [17], was imaged in noncontact mode using a Park Scientific Autoprobe CP with a  $512 \times 512$  resolution.

Figs. 2 and 3 show the AFM images of two of the Si spikes on the tip-characterization sample scanned by Si-tip and tube-tip, respectively. In both cases, the images were obtained after scanning of the sputtered-Si samples was complete (see Section 3). The characterization of the tips makes use of the convolution of tip-shape and surface morphology inherent in AFM work [5,6]. When scanning an isolated structure that is much sharper

than the probe, the resulting image is essentially a scan of the probe itself. The silicon spikes of the characterization array have a nominal tip radius of  $<10$  nm, which is comparable to the nominal Ultralever tip radius specified by TM microscopes and to experimental values for typical MWNT radii [13]. Hence, probe dimensions obtained from this technique will be overestimates (by possibly a factor of two). However, as the true dimension of the characterization spikes is unknown, these estimates represent our best guess.

For the Si-tip (Fig. 2), the image is extremely lumpy and elongated, reflecting the complex structure of the Si-tip. It is possible that the tip has fragmented or picked up some debris during scanning. Also, since the image is a convolution of both the probe and the spike, it is possible that a good deal of the structure comes from the spike itself. However, this cannot be confirmed, as there is no position indicator on the sample for relocating the spike. There is one lump that rises above the rest (shown circled in Fig. 2a and b), forming a rounded apex. This lump is assumed to be the probing region of the tip when the surface features vary in height by  $<10$  nm (the height difference from the nearest neighbor lump to the apex). It is somewhat oblong, but one side drops away more quickly than the other, indicating a nominal probe diameter of  $\sim 46$  nm corresponding to  $\gamma = 4.6$ . For larger-height variations ( $>10$  nm), more of the tip becomes involved, and the nominal probe radius quickly exceeds 100 nm.

For the tube-tip (Fig. 3), the image is more difficult to explain, though less complex. The increasing slope of the left side of the major feature seems to follow the morphology indicated in the grid specifications. The characterization spike has an initially gentle slope that quickly increases to the apex, much the same as a standard etched-Si AFM tip, like the Ultralever<sup>TM</sup>. To the right the gentle slope of the major feature may be due to the angle of approach of the nanotube, as shown exaggerated in the inset of Fig. 3a. As the probe approaches from the left, it presents a sharper profile, as the apex of the nanotube interacts with the gentle slope of the spike. As the probe passes the apex of the spike, the side of the nanotube becomes the probing region. As the probe moves

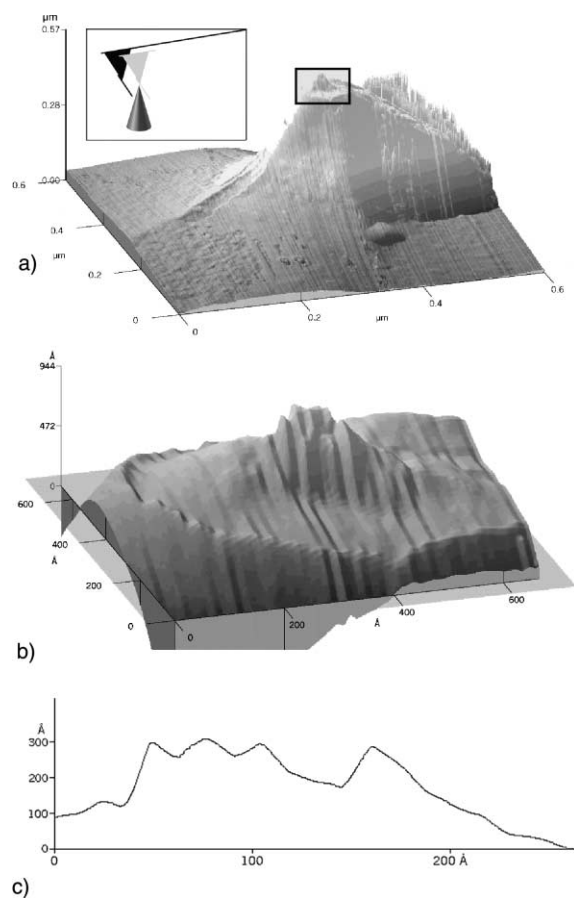


Fig. 3. Micrograph of a silicon characterization spike imaged with the tube-tip. (a) A 3-D projection of the topography. The inset, a depiction of the tube-tip scanning a stylized spike, is described fully in the text. (b) Zoomed-in 3-D topography of the peak region enclosed in a rectangle. (c) A cross-section of the central peaks in (b).

further to the right, it interacts with the spike apex further along the nanotube's length. In this case, the spike, being sharper than the side-on nanotube, essentially becomes the imaging probe. Once it is far enough away from the spike, the apex of the nanotube will again become the probing region.

The fine structure at the image apex, resembling an island (rectangled region of Fig. 3a shown zoomed in Fig. 3b), is possibly due to imaging of the characterization spike with a protruding inner shell of the MWNT. The striations in this region are due at least partly to the interpolation between

scan lines, though some of the fine structure may be real. Fig. 3c shows a cross-section through the long axis of the peak feature. Viewed from the top, this feature is roughly rectangular, with a length of  $\sim 16$  nm, a width of  $\sim 12$  nm and a height above the flatter regions of  $\sim 18$  nm, corresponding to  $\gamma = 0.78$ . As the nominal width and height of this portion of the tip are much larger than the 5 nm resolution mentioned before, it is likely that the smaller peaks in the fine structure represent real extensions of inner shells of the nanotube. The width of the uppermost peak is  $\sim 5$  nm and it rises roughly 5 nm above the nearest neighbor peak.

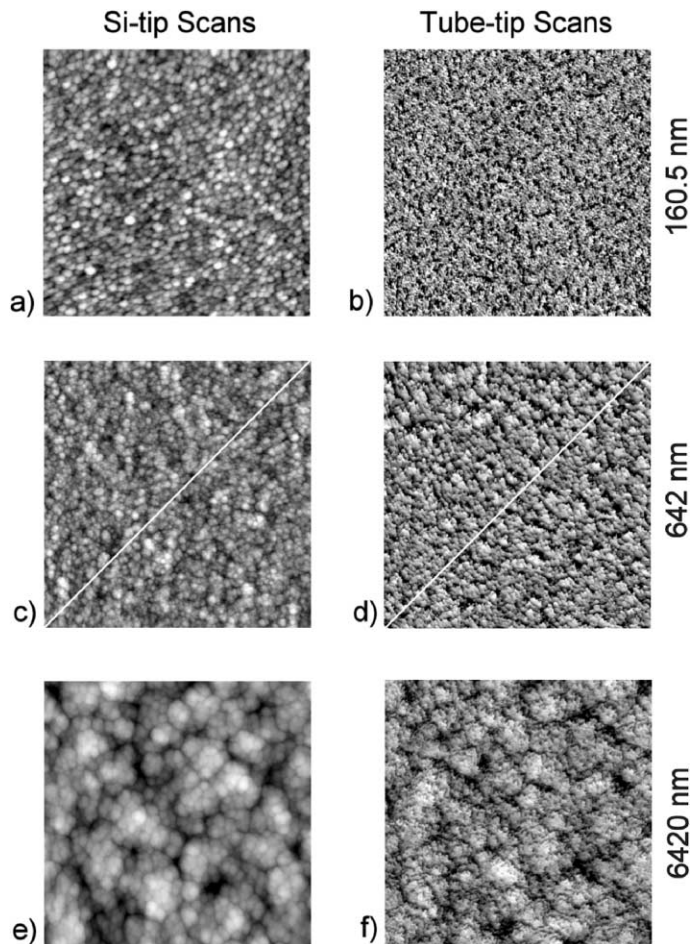


Fig. 4. Some representative surface images ( $1 \mu\text{m} \times 1 \mu\text{m}$ ) of the sputtered-silicon films scanned with both a conventional silicon AFM probe (a,c,e) and a nanotube-enhanced probe (b,d,f). The numbers on the right of the images are nominal film thicknesses. The white diagonal lines in (c) and (d) represent the cross-sectional plots shown in Fig. 5.

These dimensions could account for the observed post-attachment resolution of the tube-tip.

### 3. Characterization of sputtered-Si growth fronts

In order to estimate how the tip resolution affects the determination of growth mechanism, we have performed AFM scans on a series of DC-sputtered amorphous Si films that have been previously studied by contact mode AFM with a standard  $\text{Si}_3\text{N}_4$  tip [18]. The sample preparation conditions are described in detail in Ref. [18]. The samples range in thickness from 53.5 to 6420 nm.

The seven sample surfaces were imaged with noncontact AFM, using a Park Scientific Auto-probe CP with a  $512 \times 512$  resolution and a  $1 \mu\text{m}$  scan size. For imaging, we used both the tube-tip and several Si-tips as mentioned previously in Section 2. To characterize the surfaces of the sputtered-silicon films, a sequence of a minimum of fourteen (and a maximum of thirty) AFM images was captured for each sample. Multiple images of several regions on each sample were scanned. These images were then processed with a second order, line-by-line flattening routine, for consistency between images. For each processed image, the 1-D average height–height correlation function,  $H(x)$ , and the 2-D autocovariance function,  $G(r)$ , were calculated [4]. The data for  $H(x)$  and  $G(r)$  were then averaged for each sample.

Fig. 4 presents six micrographs of three of the seven samples, half made with various Si-tips, half with the tube-tip. Upon comparison of the images, a striking qualitative difference is immediately evident. It is obvious that the lateral resolution is many times better for the tube-tip scans. It can also be seen from the images that the intergrain boundaries are much deeper in the tube-tip images. Shown, in Fig. 5, are cross-sections corresponding to the white diagonals in Fig. 4c and d, the two 642 nm deposition images. These cross-sections serve to illustrate the enhancement of both lateral and vertical resolution. Not only is the average grain size visibly smaller for the tube-tip cross-section, but also the transitions from peak to trough are sharper and the troughs are much deeper.

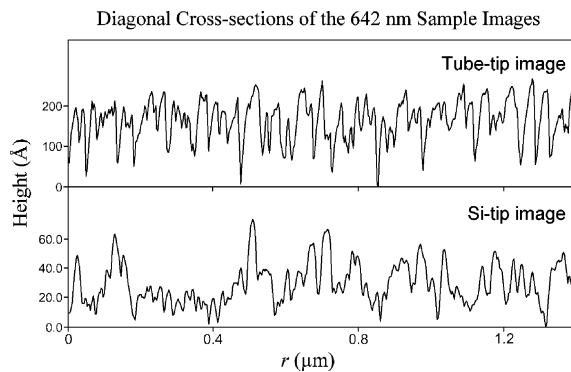


Fig. 5. Diagonal cross-sections of Fig. 4c and d, for the 642 nm deposition. Not only is the average grain size visibly smaller for the tube-tip cross-section, but the transitions from peak to trough are sharper and the troughs are much deeper.

## 4. Results

### 4.1. Roughness exponent

Aué and De Hosson have shown that the dilation process that decouples the vertical and lateral tip-surface interactions, causes an underestimation of the fractal dimension,  $D_s$ , and hence an overestimation of  $\alpha$ , for probes of nonzero aspect ratio [6]. The roughness exponent,  $\alpha$ , describes how jagged a surface is, on length scales smaller than  $\xi$ , where smaller values of  $\alpha$  correspond to more jagged surfaces, and is related to the fractal dimension by  $\alpha = 3 - D_s$ . It is to be expected, then, that the tube-tip, which should have a much lower-aspect ratio than the Si-tip over large length scales, should produce images with a smaller value of  $\alpha$ .

To obtain values for  $\alpha$ , the 1-D average height–height correlation function,  $H(x)$ , was taken for each image of a given sample.<sup>2</sup> These  $H(x)$  were then averaged, and fit to a power law in  $2\alpha$ , for  $x < \xi$ . Fig. 6 is a plot of the average  $H(x)$  for the seven samples showing data from both the tube-tip and the Si-tip. Fig. 7 shows a plot of the roughness exponents for the seven samples. The square data points correspond to the Si-tip image data, the

<sup>2</sup> The 1-D average  $H(x)$  is obtained from the average of  $H(x)$  for each line of the image in the fast scan direction. This function is equivalent to the 2-D circularly averaged  $H(r)$  due to the isotropy of the films [18].

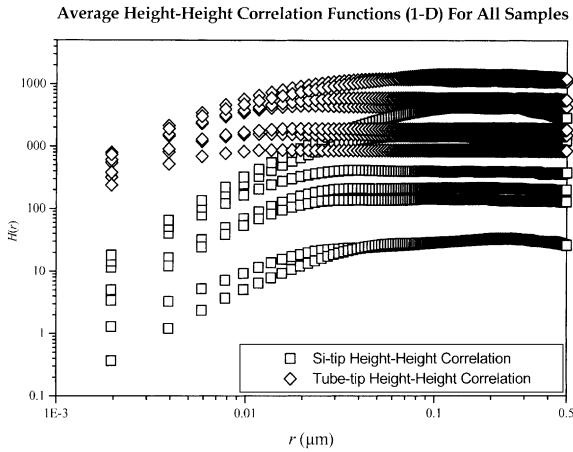


Fig. 6. The average 1-D height–height correlation functions for all of the samples, obtained from both the tube-tip and conventional tips.

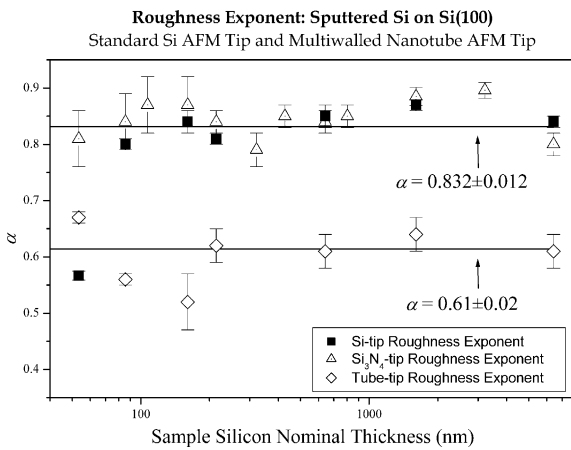


Fig. 7. Roughness exponent,  $\alpha$ , versus sample thickness for sputtered-silicon scanned with both a conventional silicon AFM probe and the MWNT probe. Lines indicate the weighted averages of the data. Shown for comparison are the  $\alpha$  values from the data presented in Ref. [18] with average  $0.83 \pm 0.03$ .

open diamonds to the tube-tip, and the dotted triangles to the values reported in Ref. [18]. For all samples, except the 53.5 nm one, the values of  $\alpha$  obtained with the tube-tip are  $\sim 0.2$  lower than those obtained from the standard-probe scans. The anomalous dip of the Si-tip  $\alpha$  data for the 53.5 nm sample is not understood.

As predicted by Aué and De Hosson [6], the lower-aspect-ratio tube-tip produces images with

much smaller values of  $\alpha$ . A common problem during AFM scanning, which occurs even for noncontact mode, is the degradation of the probe tip. The tip may pick up debris, be blunted, or break off. This effect contributes to the increase in  $\alpha$ , through the decrease of  $d$  or  $\gamma$ . For our work, though we did see a small loss of resolution due to tip degradation while scanning with the Si-tips, even initial scans with fresh tips produced larger values of  $\alpha$ . The tube-tip showed no such degradation.

#### 4.2. Lateral correlation length

To obtain  $\xi$  for the samples, the 2-D autocovariance function,  $G(r)$ , was calculated for each image. These data were then averaged for each sample, and  $\xi$  was determined graphically from the value of  $r$  at  $G(\xi) = G(0)/e$ . Fig. 8 presents the results of these calculations, with the Si-tip data in squares, the tube-tip data in open diamonds, and the  $\text{Si}_3\text{N}_4$ -tip data from Ref. [18] in dotted triangles. The value of  $\xi$  is significantly and consistently lower as derived from the tube-tip images than as derived from the Si-tip images. It would seem the tube-tip’s enhanced resolution enables it to resolve shorter-length-scale correlations. Both standard-probe curves show a flattening, or saturation, at short growth times (dashed line in Fig. 8). This effect supports the notion that the tube-tip is able

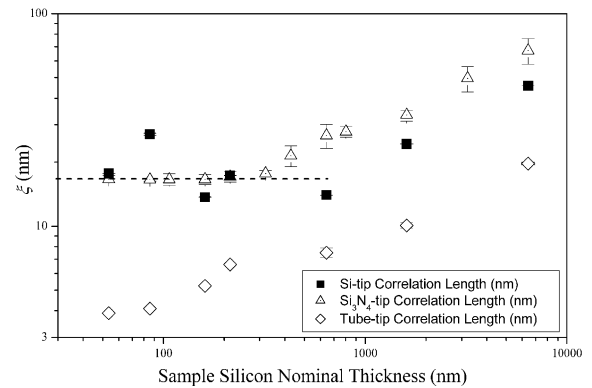


Fig. 8. Lateral correlation length,  $\xi$ , versus sample thickness for images obtained with both a conventional silicon AFM probe and the MWNT probe. Also shown are  $\xi$  values reported in Ref. [18] for contact mode AFM.

to resolve smaller features and therefore shorter-length correlations.

## 5. Conclusion

We have presented a study of the adequacy of nanotube AFM probes for obtaining surface morphology statistics as compared to conventional etched-silicon or  $\text{Si}_3\text{N}_4$  probes. We have shown that nanotube AFM probe tips may provide an advantage over conventional probes when obtaining values for roughness coefficient,  $\alpha$ , and lateral correlation length,  $\xi$ . The average value for the roughness exponent,  $\alpha = 0.61 \pm 0.02$ , obtained from the noncontact tube-tip images is  $\sim 0.2$  smaller than those from the standard tips in both contact and noncontact modes, and more closely approaches the intrinsic value for the surfaces. Values for the lateral correlation length,  $\xi$ , are also consistently smaller when calculated from tube-tip images, possibly reflecting shorter correlation lengths made apparent by the higher lateral resolution.

We would like to caution the reader that there are concerns that arise from the intrinsic properties of the nanotube probe. For example, as mentioned in Section 2, the nanotube is not extended perpendicular to the cantilever, but is at an angle partially controlled by the angle of the silicon pyramid. This enhanced angle of attack has been shown to provide a ‘tip artifact’ as evident in the difference in slope of the two sides of the characterization spike discussed in Section 2. Such tip artifacts may have a deleterious effect on the calculation of surface statistics for samples with large-height changes.

Another complication is the sensitivity of AFM probes to feedback set points. Upon approaching the surface too closely, noise spikes appear in the images as the probe interacts with large-height changes in topography. At the high lateral resolution of the tube-tip probe, it becomes increasingly difficult to visually detect such spikes, which can greatly increase the calculated interface width of an image. To address the aforementioned complications, we propose to perform more tube-tip scans on this and other systems with time dependent surface roughness, using other nanotube

probes. More work is needed, before a definitive statement can be made about the efficacy of tube-tip probes for measuring growth-/etch-front roughness parameters.

## Acknowledgements

The authors would like to thank Dr. Anthony Chan for the use of his software, STMCalc, in calculating  $H(r)$  and  $G(r)$ . This work was supported in part by NSF DMR. C.V.N. was supported by a contract from NASA Ames to ELORET Corporation.

## References

- [1] A.-L. Barabási, H.E. Stanley, *Fractal Concepts in Surface Growth*, Cambridge University Press, Cambridge, England, 1995.
- [2] P. Meakin, *Fractals, Scaling, and Growth Far from Equilibrium*, Cambridge University Press, Cambridge, England, 1998.
- [3] F. Family, T. Viscek, *Dynamics of Fractal Surfaces*, World Scientific, Singapore, 1991.
- [4] Y.-P. Zhao, G.-C. Wang, T.-M. Lu, *Characterization of Amorphous and Crystalline Rough Surfaces: Principles and Applications*, Academic Press, San Diego, 2001.
- [5] D. Keller, *Surf. Sci.* 253 (1991) 353.
- [6] J. Aué, J.T.M. De Hosson, *Appl. Phys. Lett.* 71 (1997) 1347.
- [7] TM Microscopes, Ultralevers™: Maximum Resolution Cantilevers, 1999. Available from <<http://www.tmmicro.com/products/probepdf/ultra.pdf>>.
- [8] TappingMode AFM Probes, 2001. Available from <<http://www.di.com/products2/NewProbeGuide/TappingModeProbes.html#NanosensorsEtched>>.
- [9] General Description of Pointprobes, 2001. Available from <<http://molec.com/products/consumables/nanosensors/general.html>>.
- [10] High ART Tapping Probes, 2001. Available from <<http://www.di.com/products2/NewProbeGuide/HighARTappingProbes.html>>.
- [11] G. Nagy, M. Levy, R. Scarmozzino, J.R.M. Osgood, *Appl. Phys. Lett.* 73 (1998) 529.
- [12] C.V. Nguyen, K.-J. Chao, R.M.D. Stevens, L. Delzeit, A. Cassell, J. Han, M. Meyyappan, *Nanotechnology* 12 (2001) 363.
- [13] S.S. Wong, A.T. Woolley, T.W. Odom, J.-L. Huang, K. Philip, *Appl. Phys. Lett.* 73 (1998) 3465.
- [14] Y. Nakayama, H. Nishijima, S. Akita, K.I. Hohmura, S.H. Yoshimura, K. Takeyasu, *J. Vac. Sci. Technol. B* 18 (2000) 661.

- [15] R.M.D. Stevens, C.V. Nguyen, A. Cassell, L. Delzeit, M. Meyyappan, J. Han, *Appl. Phys. Lett.* 77 (2000) 3453.
- [16] R.M.D. Stevens, N.A. Frederick, B.L. Smith, D.E. Morse, G.D. Stucky, P.K. Hansma, *Nanotechnology* 11 (2000) 1.
- [17] MikroMasch, MikroMasch calibration gratings for SPM, 2001. Available from <[http://www.spmtips.com/products/grat\\_soft/tgt01.htm](http://www.spmtips.com/products/grat_soft/tgt01.htm)>.
- [18] T. Karabacak, Y.-P. Zhao, G.-C. Wang, T.-M. Lu, *Phys. Rev. B* 64 (2001) 085323.